Electron and Photon Performance Measurements with the ATLAS Detector

Dimitra Tsionou
Laboratoire d Annecy-le-Vieux de Physique des Particules
& University of Sheffield
on behalf of the ATLAS Collaboration

Abstract

At LHC, excellent particle reconstruction and identification is needed for electrons and photons. The measurement of the electron and photon performance and the determination of the electromagnetic energy scale are presented using proton-proton collision data collected in 2010/2011. The electron and photon identification and isolation requirements are described and their efficiency rates are discussed.

1 Introduction

The precise measurement of the electron and photon performance with the ATLAS detector at the LHC is vital not only for the measurement of Standard Model processes but also for searches including the Higgs boson. These processes produce particles with energy range from a few GeV to a few TeV. To distinguish isolated electrons and photons from background objects such as hadron jets, excellent electron and photon identification is needed. In order to achieve this, a combination of the ATLAS subdetectors [1] is exploited: the inner detector (ID) is used to separate electrons and photons and to measure the tracks associated to electrons and converted photons; the electromagnetic calorimeter (EMC) measures the energy and position of the electromagnetic showers; the hadronic calorimeter is used to measure the leakage of the electromagnetic shower behind the electromagnetic calorimeter.

2 Improved Electron Reconstruction Using Gaussian Sum Filter-based model for bremsstrahlung

The behaviour of high-energy electrons in the ATLAS ID is dominated by radiative energy losses (bremsstrahlung) when interacting with the material. These losses can be significant and can give rise to deviations from the original charged particles path,

resulting in alterations of the curvature of the electrons trajectory in the magnetic field. The ATLAS electron reconstruction has been improved to take into account such radiative losses by using track refitting with the Gaussian Sum Filter (GSF) algorithm in order to improve the estimated electron track parameters [2]. Figure 1 shows the improvement on the track parameters for high and low p_T electrons, in simulation and data respectively.

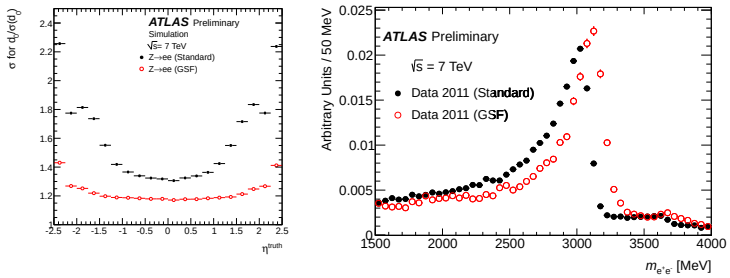

Figure 1: *Left plot:* The dependence on the pseudorapidity η of the width of the transverse impact parameter significance for GSF (open red) and standard (solid black) truth-matched Monte-Carlo electrons from Z-boson decays. *Right plot:* The e^+e^- invariant mass distributions for prompt J/ψ 2011 collision data samples [2].

3 Energy Scale and Resolution

An in-situ calibration is used in ATLAS to fine tune the electromagnetic energy scale provided by the EMC on data. The well-known mass of the Z boson and its decay in e^+e^- pairs are used to improve the knowledge of the electron energy scale and the linearity of the electromagnetic calorimeter. In addition, the J/ψ process as well as the $W \to e\nu$ (the latter relying on an E/p measurement) are also used to cross-check the obtained results. For the $Z \to ee$ channel, two electrons with transverse energy $E_T > 20$ GeV are required to satisfy an invariant dielectron mass in the range 80-100 GeV, in the pseudorapidity region $|\eta| < 4.9$.

To determine the energy scale, the electron energy is parametrised as $E^{meas} = E^{true}(1+\alpha_i)$ for a given region i, where E^{meas} is the energy measured by the calorimeter after a simulation based energy scale correction, E^{true} is the true electron energy and α_i the residual miscalibration. The energy scale correction factors α are determined using a log-likelihood fit and constraining the dielectron mass to the Z boson lineshape. Figure 2 shows the α correction factors as a function of the pseudorapidity for the region $|\eta| < 4.9$ and its stability over time. The main systematic uncertainties on the electron energy scale (at the level of 1% each) are coming from the knowledge

of the material budget in the simulation setup, from the uncertainty in the description of the low E_T electrons, and from the presampler energy scale [3].

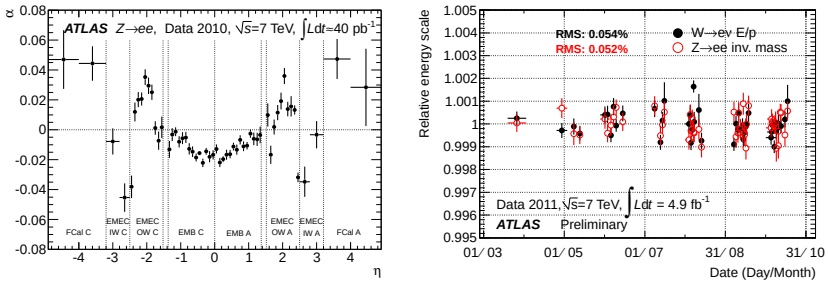

Figure 2: *Left plot:* The energy-scale correction factor α as a function of the pseudo-rapidity of the electron cluster derived from fits to $Z \to ee$ data. The uncertainties of the $Z \to ee$ measurement are statistical only. The boundaries of the different detector parts are indicated by dotted lines [3]. *Right plot:* Energy scale obtained by the $Z \to ee$ (black points) and $W \to e\nu$ (red points) method presented as a function of time. The values obtained by these two methods are normalised to one. Each point represents a recorded amount of data of around 100 pb^{-1}. The quoted RMS is the sum of statistical fluctuations and time dependence, providing an upper bound on the energy response uniformity with time [4].

4 Electron and Photon Identification

The electron and photon identification provides good separation of isolated electrons and photons from background objects (non-isolated electrons, background electrons from photon conversions and Dalitz decays, hadron jets, non-prompt photons from the decay of neutral hadrons in jets, ...). The requirements of the electron and photon identification for the central region $|\eta| < 2.5$ include lateral and longitudinal shower shape variables using information from the different layers of the electromagnetic calorimeter and energy leakage in the hadronic calorimeter. In addition, for the electrons track quality variables and cluster-track matching information are also used.

There are three levels of electron identification called loose, medium and tight each with more stringent requirements. For photons two identification levels are defined: loose and tight.

In the forward region ($2.5 < |\eta| < 4.9$) where there are no tracking detectors present, the identification relies solely on cluster moments and shower shapes. These provide efficient discrimination against hadrons due to the good transverse and longitudinal segmentation of the calorimeters, though it is not possible to distinguish

between electrons and photons. Two identification levels are defined in this case: forward loose and forward tight.

4.1 Electron Identification Measurements

The measurements of the electron identification efficiencies are performed using the Tag-and-Probe method. This method uses W, Z and J/ψ decays in electrons to derive data-driven efficiency measurements. It is based on the definition of a probe-like object, used to make the performance measurement, within a properly tagged sample of events. In the following, a well-identified electron is used as the tag in the $Z \to ee$ and $J/\psi \to ee$ measurements and high missing transverse momentum is used in the $W \to e\nu$ measurements.

For these measurements, the contamination of the probe sample by background requires the use of some background estimation technique (usually a side-band or a template fit method on the dielectron mass for Z and J/ψ measurements or the isolation distribution for the W measurements). The number of electron candidates is then independently estimated both at the probe level and at the level where the probe passes the cut of interest. The efficiency is equivalent to the fraction of probe candidates passing the cut of interest.

The efficiency measurements for the medium and tight identification performed using the $W \to e\nu$ Tag and Probe method are shown in Figure 3 as a function of the pseudorapidity and integrated for electrons with transverse energy $20 < E_T < 50$ GeV. With this method, the E_T region between 15-20 GeV is also explored. Compatible results are obtained with the $Z \to ee$ Tag and probe method used in the E_T region 20-50 GeV and the J/ψ method is used for low-E_T electrons ($4 < E_T < 20$ GeV). For the Z and J/ψ measurements, the statistical uncertainty is comparable to the systematics. The main sources of systematic uncertainties are the background subtraction method, the discriminating variable used and the level of the background contamination.

The dependence of the electron identification efficiencies for all three identification levels on the number of reconstructed vertices during the 2011 data taking is shown in Figure 4. The number of reconstructed vertices is a way to assess the in-time pileup. Alterations to the identification requirements have been made in preparation for the 2012 data taking in order to provide a more robust behaviour against pileup.

4.2 Photon Identification

Unlike the electron case, the method presented here in order to measure the identification efficiency for photons is not completely data-driven. The photon identification efficiencies are measured in simulation samples and are then corrected for differences observed between simulation and data. An important requirement used in photon

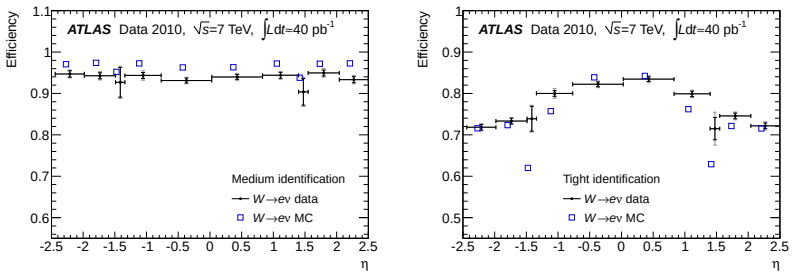

Figure 3: Electron identification efficiencies measured on $W \to e\nu$ events and predicted by Monte Carlo for (left) medium and (right) tight identification as a function of η and integrated over $20 < E_T < 50$ GeV. The results for the data are shown with their statistical (inner error bars) and total (outer error bars) uncertainties. The statistical error on the Monte Carlo efficiencies plotted as open squares is negligible. For clarity, the data and Monte Carlo points are slightly displaced horizontally in opposite directions [3].

analyses is the isolation of the photon candidate defined as the transverse energy deposit within a cone around the calorimetric photon cluster.

The first plot in Figure 5 shows the tight photon identification efficiencies measured as a function of the reconstructed transverse energy in three different pseudorapidity bins. The identification efficiency increases for higher E_T from the level of 65% for the E_T region 15-20 GeV to 95% for photons with transverse energy $60 < E_T < 100$ GeV [6]. The second plot shows the photon isolation distribution for the leading photon as measured for a diphoton analysis. The variable E_T^{iso} is calculated by summing the cells of the electromagnetic and hadronic calorimeters in

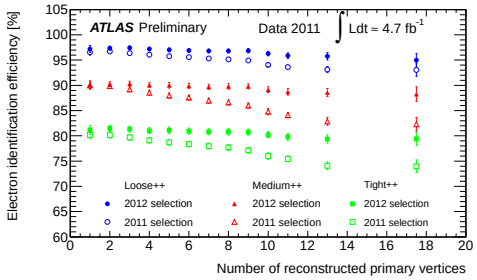

Figure 4: Identification efficiencies as a function of the number of reconstructed vertices during the 2011 data taking (open circles) and as expected for the 2012 data (dark circles) after reoptimisation of the identification requirements [5].

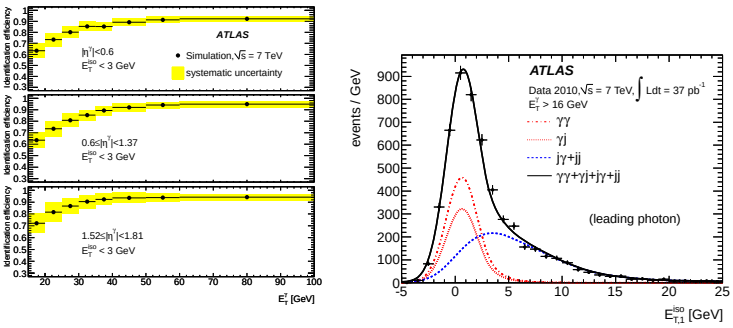

Figure 5: *Left plot:* Tight identification efficiency as a function of the reconstructed photon transverse energy for prompt isolated photons in three different pseudorapidity regions. The efficiency is calculated with respect to reconstructed true photons satisfying $E_T^{iso} < 3$ GeV. The yellow bands include the systematic uncertainties [6]. *Right plot:* Isolation distribution for the leading photon in diphoton events. The solid points represent the data, the black solid line indicates the fit result and the dash-dotted curves show the diphoton decomposition [7].

a cone of angular radius $R < 0.4$ around the photon candidate. The E_T^{iso} is corrected to take into account the energy leakage outside the photon cluster and the ambient energy density measured in the event [7].

References

[1] ATLAS Collaboration, The ATLAS Experiment at the CERN Large Hadron Collider, JINST 3 S08003, 2008.

[2] ATLAS Collaboration, Improved electron reconstruction in ATLAS using the Gaussian Sum Filter-based model for bremsstrahlung, ATLAS-CONF-2012-047.

[3] ATLAS Collaboration, Electron performance measurements with the ATLAS detector using the 2010 LHC proton-proton collision data, Eur. Phys. J. C (2012) 72:1909.

[4] ATLAS Collaboration, Plots on electron energy response stability with time and pile-up, ATL-COM-PHYS-2012-259.

[5] ATLAS Collaboration, Electron identification efficiency dependence on pileup (update), ATL-COM-PHYS-2012-260.

[6] ATLAS Collaboration, Measurement of the inclusive isolated prompt photon cross section in pp collisions at $\sqrt{(}s) = 7$ TeV with the ATLAS detector, Phys.Rev. D83 (2011) 052005.

[7] ATLAS Collaboration, Measurement of the isolated diphoton cross section in pp collisions at $\sqrt{(}s) = 7$ TeV with the ATLAS detector, Phys. Rev. D85 (2012) 012003.